Small Molecules Targeting Fyn Kinase as Potential Therapies for Alzheimer's Disease

Xinyue Liu[1]

Received August 14, 2026
Accepted October 21, 2026
Electronic access November 30, 2026

Alzheimer's disease (AD) is a progressive neurodegenerative disorder characterized by the accumulation of amyloid-β (Aβ) plaques, intracellular tau aggregation, and progressive neuronal loss. Because AD involves multiple pathological pathways, treatments targeting a single mechanism have shown limited success. In this study, we focused on targeting Fyn kinase, a protein with connections to both the Aβ pathway and the tau pathway, making it a promising target for AD treatment. By analyzing the protein's structure using a combination of geometric and machine learning methods, we found several promising binding sites on the protein's surface. Then, a pharmacophore-based virtual screening was performed to identify small molecules with high binding affinity to Fyn kinase binding sites. The resulting compounds were then evaluated using molecular docking to predict their binding poses and approximate binding free energies (ΔG) within each binding site. The highest-scoring candidates were tested for their toxicity and absorption, distribution, metabolism, and excretion (ADME) affinity as well as overall effects on the organs and molecular pathways. These experiments identified two computational hits with predicted binding affinity with Fyn kinase, acceptable ADME properties, and acceptable predicted toxicity across organs and molecular pathways. These findings provide candidates for future experimental validation of computational drug discovery, in vitro testing, lead optimization, preclinical testing, and clinical development.

Keywords: Drug discovery, Alzheimer's disease, Virtual screening, Molecular docking, Fyn kinase

Introduction

Alzheimer's disease (AD) is the most prevalent neurodegenerative disorder that accounts for approximately 60 - 80% cases of dementia worldwide[1,2]. In the early 21st century, over 35 million people have suffered from the disease, with the number of patients expected to double over the next 20 years[3]. Clinically, AD is characterized by progressive cognitive decline, memory impairment, and deterioration in language, reasoning, and executive functioning[1,3]. Caretakers of AD patients shoulder significant burdens as they deal with the patient's various behavioral and mood symptoms[3]. Despite decades of research, therapeutic advances remain limited; currently available treatments primarily provide symptomatic relief rather than controlling disease progression[1,2].

Pathological hallmarks of AD include the extracellular accumulation of β-amyloid (Aβ) plaques and the intracellular aggregation of hyperphosphorylated tau protein into neurofibrillary tangles (NFTs)[1,2]. Improper cleaving of APP by β and γ-secretase produces insoluble Aβ peptides that accumulate due to an imbalance between their production and removal[4]. According to the amyloid cascade hypothesis, abnormal Aβ accumulation initiates a sequence of neurotoxic events that promote synaptic dysfunction, neuronal death, and prolonged gliosis[5]. Concurrently, insoluble deposits of misfolded tau aggregate in the cell body and dendrites of neurons[6]. Tau pathology disrupts microtubule stability and axonal transport, accelerating neurodegeneration and cognitive decline[2,7]. The accumulation of Aβ plaques and NFTs is closely associated with AD progression cognitive decline, emphasizing the importance of identifying molecular pathways responsible for the buildup of tau and Aβ[8].

Several therapeutic pathways have emerged as major targets for AD treatment. The amyloid pathway primarily focuses on reducing Aβ production, aggregation, or deposition through immunotherapies and enzyme-targeting approaches[9]. Tau-directed therapies seek to prevent tau hyperphosphorylation and aggregation into NFTs[10]. Neuroinflammation has also become an important therapeutic target because activated microglia and astrocytes contribute to chronic inflammatory responses that exacerbate neuronal injury[11,12]. Current pharmacological treatments for Alzheimer's disease primarily include cholinesterase inhibitors and memantine, which are used to alleviate symptoms and delay cognitive decline rather than directly target the underlying disease pathology[13,14]. However, because all of these pathways appear in AD patients, single-

[1] *Basis Independent Silicon Valley*

© The National High School Journal of Science 2026

pathway interventions experienced limited success, suggesting that therapies targeting multiple pathways may provide greater clinical benefit[15].

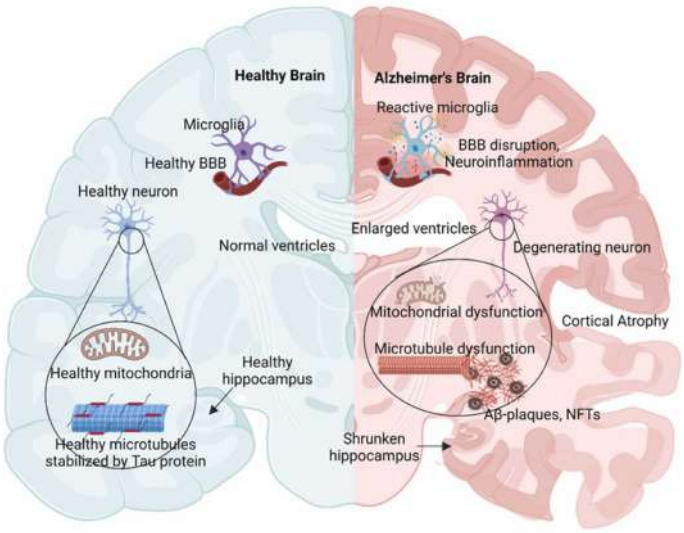


Figure. 1 Hallmarks and biological pathways of AD. Biological pathways like Aβ aggregation, tau hyperphosphorylation, neuroinflammation, etc. contribute to disease progression. Hallmarks of the disease include Aβ-plaques, p-tau, NFTs, and anatomical changes like enlarged ventricles, cortical atrophy, and shrunken hippocampus[7].

One promising target is Fyn kinase, a member of the Src family of non-receptor tyrosine kinases. Fyn is highly expressed throughout the central nervous system, particularly within the hippocampus and cerebral cortex[16,17]. Under normal physiological conditions, Fyn kinase regulates neuronal development, synaptic plasticity, neurotransmitter signaling, and long-term potentiation through interactions with N-methyl-D-aspartate (NMDA) receptors[16,18]. Fyn kinase has three isoforms that perform various functions throughout the body. While Fyn-B is highly expressed in the brain and contributes to neuronal functions, Fyn-T is predominantly expressed in hematopoietic cells, whereas Fyn-Δ7 is primarily expressed in peripheral blood mononuclear cells[19]. This presents a difficulty in targeted treatment as inhibiting Fyn kinase function could cause unintended consequences throughout the body[20].

Accumulating evidence suggests that Fyn kinase signaling plays a central role in Alzheimer's disease progression. Fyn mediates Aβ-induced synaptic dysfunction through aberrant NMDA receptor signaling, and additionally interacts with tau to promote synaptic degeneration. Fyn also contributes to neuroinflammation by regulating microglial activation, allowing the protein to affect major pathological processes underlying AD[21,22]. Dysfunctional microglia and chronic neuroinflammation are additionally associated with tau pathology and its progression in AD[23]. Thus, Fyn acts as a critical intermediary between Aβ and tau pathology, with Aβ-induced Fyn activation promoting tau phosphorylation and Fyn recruitment to postsynaptic NMDA receptors, where Fyn-mediated NR2B phosphorylation contributes to excitotoxic synaptic signaling[24,25].

In this study, we aim to use computational drug discovery methods to identify potential small molecule therapeutics targeting Fyn kinase for the treatment of AD. The experimental workflow includes binding pocket prediction, pharmacophore-based virtual screening, molecular docking, ADME prediction, and toxicity prediction. Experimental validation, including in vitro, in vivo, and clinical studies, is beyond the scope of this work. Additionally, the results depend on the accuracy of the computational models used and available molecular databases, which may not fully capture biological complexity.

Methods

DoGSiteScorer

Potential binding sites on the Fyn kinase structure were evaluated for their suitability for small-molecule ligands based on their geometric and structural properties, including pocket volume, surface area, shape, depth, enclosure, and drug score. Suitable binding pockets were expected to have appropriate volumes consistent with small-molecule binding sites. Larger surface areas, appropriate pocket depth, and sufficient enclosure were also considered when evaluating potential binding sites.

Binding sites were analyzed with the DoGSiteScorer tool available on `https://proteins.plus/`, using the Pocket(s) analysis option and druggability granularity setting enabled. Calculations were carried out on both protein chains. The DoGSiteScorer algorithm applies a geometric approach to evaluate binding pockets, generating drug scores based on structural elements such as volume, surface area, depth, and enclosure. The purpose of this experiment was to evaluate the suitability of Fyn kinase as a target for small-molecule binding, rather than to characterize individual binding sites.

PrankWeb

To complement geometric analysis, binding sites were further evaluated using PrankWeb (`https://prankweb.cz/`) which uses a machine-learning-based approach to account for both the geometry and energetic favorability of a binding site. Energetic favorability reflects the thermodynamic likelihood of ligand binding and is related to the decrease in free energy when a ligand binds to a pocket. Calculations were performed

© The National High School Journal of Science 2026

with an Experimental structure input method, with use of original structure and conservation enabled.

Virtual Screening

Virtual screening was performed using the Pharmit platform (`https://pharmit.csb.pitt.edu/`). The crystal structure of the human Fyn kinase domain (PDB ID: 10DJ; UniProt P06241) was used to generate a pharmacophore-based screening model. This structure represents an active-like form of Fyn kinase and was therefore selected as a suitable structure for evaluating small-molecule binding. The structural state was selected because it represents the catalytically competent form of Fyn and therefore proves a relevant model for screening potential kinase inhibitors. The pharmacophore map was derived from the interactions between the co-crystallized ligand saracatinib (H8H), a known Fyn inhibitor, and the Fyn kinase binding site. Binding-site water molecules were ignored for the virtual screening, but they were taken into account for the subsequent molecular docking experiment for more accurate results. The screening was done on Pocket 2 on chain A of Fyn kinase.

Two pharmacophore maps were selected for virtual screening as shown in Figure 2. Map A contained two HydrogenAcceptor and two Hydrophobic interactions. Map B contained the same four features as Map A, with an additional Hydrophobic interaction.

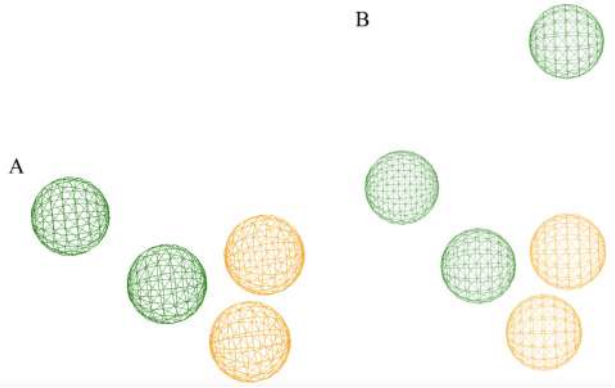


Figure. 2 Visualization of the two pharmacophore maps used. A) Map A featuring two HydrogenAcceptor features (in yellow) and two Hydrophobic features (in green). B) Map B featuring two HydrogenAcceptor features (in yellow) and three Hydrophobic features (in green). Each feature has a radius of 1.0 Å.

The specific coordinates and radii of each map feature are shown below in Table 1.

The screening was performed over the MolPort and Enamine compound databases. Candidate molecules were ranked according to their RMSD score (root mean square of deviation), indicating their compatibility with the defined pharmacophore. The 30 highest-ranked candidate molecules selected from the virtual screening stage were retained for subsequent molecular docking.

Table 1. Pharmacophore features and coordinates used in virtual screening. Specific pharmacophore features used in the pharmacophore maps, including their Cartesian (x, y, z) coordinates and corresponding radii.

Map	Feature	x (Å)	y (Å)	z (Å)	Radius (Å)
A	HydrogenAcceptor	-13.3	15.7	-14.3	1.0
A	HydrogenAcceptor	14.3	15.0	-16.1	1.0
A	Hydrophobic	-14.1	13.3	-14.2	1.0
A	Hydrophobic	-13.8	11.3	-11.9	1.0
B	HydrogenAcceptor	-13.3	15.7	-14.3	1.0
B	HydrogenAcceptor	14.3	15.0	-16.1	1.0
B	Hydrophobic	-11.6	15.9	-8.9	1.0
B	Hydrophobic	-14.1	13.3	-14.2	1.0
B	Hydrophobic	-13.8	11.3	-11.9	1.0

Molecular Docking

The 30 molecules identified through virtual screening were further tested through a molecular docking experiment using SwissDock (`https://swissdock.ch/`)[26,27]. Each ligand underwent blind docking across the entire surface of Fyn kinase, with the co-crystallized saracatinib ligand removed. SwissDock automatically repairs missing atoms and protonation states. Chain A and B were considered separately due to the size of the Fyn kinase protein and the limitations of the SwissDock server. The docking parameters for chain A are (-20,7,-7) for box center and (38,55,54) for box size. The docking parameters for chain B are (-18,-30,-37) for box center and (37,54,57) for box size. No heteroatoms were kept and the number of Random Initial Conditions (RIC) generated was 1.

Docking results were evaluated according to the predicted docking score reported by SwissDock. The best-performing result for each ligand across two protein chains was recorded. The docking results were used to filter the initial 30 compounds to 15 candidates based on their SwissDock scores, , not to necessarily rank the compounds.

ADME

The 15 compounds selected following molecular docking were evaluated for predicted ADME properties along with blood-brain barrier (BBB) permeability using the SwissADME server (`https://www.swissadme.ch/`). Because Alzheimer's disease is a central nervous system (CNS) disease, a small molecule intended to act in the brain generally needs to reach the CNS. Therefore, predicted BBB permeability is relevant when evaluating whether molecules are plausible CNS drug candidates. Lipinski's Rule of Five was used to

© The National High School Journal of Science 2026

assess certain molecular properties of the compounds. Lipinski compliance was assessed using the SwissADME filter.

CLogP was determined using the Consensus Log Po/w value. Water solubility was evaluated using Log S (ESOL), a topological method based on the approach described by Delaney[28]. Each compound was classified according to agreement with Lipinski's Rule of Five and BBB permeability.

Toxicity

The 13 molecules with acceptable ADME properties and were BBB permeant were then evaluated using the ProTox-3 server (`https://tox.charite.de/protox3/`). All additional models were selected to be predicted alongside acute toxicity and binding to 16 toxicity targets. The predicted LD50 and toxicity class were measured. In addition, a toxicity radar chart and a network chart were also taken.

The predicted LD50 represents the estimated dose associated with mortality in 50% of a test population. Toxicity classes ranging from 1 to 6 were recorded, with lower toxicity-class numbers representing greater predicted toxicity. The toxicity radar chart measures the compound's predicted probability as compared to the average predicted probability for active molecules in the relevant training class. A network chart indicates probability of activity and inactivity in the tested pathways. BBB permeability was kept separate from the toxicity evaluation as CNS penetration is essential for a Fyn-directed AD drug. Although BBB toxicity appears in the network charts, their effect was not considered. The toxicity analysis was not used to rank the compounds but rather to assess the extent of their effect on the human body.

Results

Binding Site Analysis using DoGSiteScorer

Using the geometric approach, DoGSiteScorer identified a total of 23 potential small-molecule binding sites on Fyn kinase as shown in Figure 3.

Table 2 presents the five highest-ranked binding sites based on drug score: P_7, P_0, P_1, P_4, and P_3.

Table 1 Properties of the five highest-ranked binding sites. Binding sites were ranked according to their drug score. Properties listed include volume (Å^3), surface area (Å^2), and drug score values. (Angstrom Å = 0.1 nm).

Name	Volume Å^3	Surface Area Å^2	Drug Score
P_7	235.8	526.91	0.74
P_0	448.18	510.21	0.73
P_1	434.2	478.68	0.70
P_4	258.19	444.01	0.61
P_3	326.97	350.49	0.59

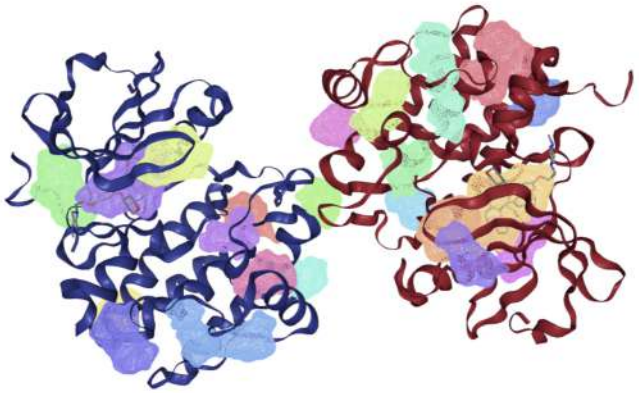


Figure. 3 Predicted small-molecule binding sites on Fyn kinase. The blue and red ribbons represent the structure of Fyn kinase. Colored spheres represent the different binding sites. A total of 23 potential binding sites were identified using this method.

As shown in Table 2, P_7 and P_0 had the highest drug scores, with values of 0.74 and 0.73, respectively. P_3 had the lowest drug score among the five sites at 0.59 and also corresponding to the lowest surface area of 350.49 Å^2. P_4 had a drug score of 0.61 despite having a moderate surface area. Overall, the analysis identified multiple potential binding regions on Fyn kinase, with P_7 and P_0 receiving the highest drug scores.

Binding Site Analysis using PrankWeb

PrankWeb identified three potential binding sites on Fyn kinase visualized in Figure 4: Pocket 1, Pocket 2, and Pocket 3.

Pocket 1 received a score of 33.55 and contained 35 residues, while Pocket 2 received a score of 29.86 and contained 33 residues as shown in Table 3. Pocket 3 had a substantially lower score of 1.57 and contained 10 residues.

Table 2 Score and number of residues of the pockets identified through PrankWeb. A higher score represents a better target for binding and a greater number of residues typically corresponds to a greater number of interactions and thus a stronger bond.

Rank ↑	Score	# of residues
1	33.55	35
2	29.86	33
3	1.57	10

Example residues identified in Pocket 1 included ASP 146, ASN 84, LEU 15, ASN 17, and SER 87. Pocket 2 included ASP 128, GLY 21, LEU 149, ASP 90, and ARG 130, while Pocket 3 included LEU 275, GLU 273, and TYR 82.

© The National High School Journal of Science 2026

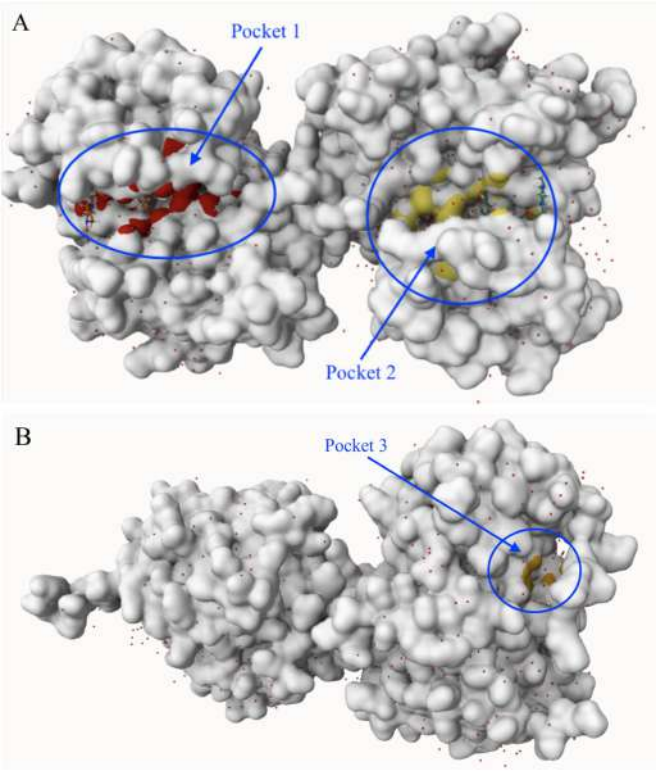


Figure. 4 Potential binding sites as identified by PrankWeb. A) The residues of Pocket 1 are shown in red, and the residues of Pocket 2 are shown in yellow. B) The residues of Pocket 3 are shown in orange.

Pharmacophore Analysis

The 30 molecules with the lowest RMSD scores were identified, along with their respective databases and an image of the interaction, as shown in Table 4.

The RMSD scores of the compounds ranged from 0.069 to 0.074 for Map A and from 0.073 to 0.111 for Map B. Using Map A, Z3015295779, MolPort-053-218-951, and MolPort-020-180-030 exhibited the lowest RMSD scores, at 0.069, 0.071, and 0.072, respectively, whereas Z1754406588 had the highest score (0.074). For Map B, Z1675272972 and MolPort-010-653-848 showed the lowest RMSD scores, at 0.073 and 0.075, respectively, while MolPort-006-846-922 had the highest score (0.111). Overall, the compounds generally exhibited lower RMSD scores with Map A than with Map B.

Molecular Docking Analysis

Molecular docking was performed on the 30 compounds identified through pharmacophore screening, identifying molecules with favorable predicted binding interactions with Fyn kinase.

SwissParam scores ranged from -6.3198 to -9.0428.

Table 3 Top 30 molecules with the lowest RMSD scores from virtual screening.

Map	Name	Database	RMSD	Image
A	Z3015295779	Enamine	0.069	
	Molport-053-218-951	Molport	0.071	
	MolPort-020-180-030	Molport	0.072	
	Molport-038-946-285	Molport	0.072	
	MolPort-044-191-483	Molport	0.072	
	MolPort-046-064-872	Molport	0.072	
	Z3015295812	Enamine	0.072	
	Z4326712495	Enamine	0.072	
	Molport-053-217-485	Molport	0.073	
	Molport-053-218-995	Molport	0.073	
	MolPort-020-168-373	Molport	0.073	
	MolPort-035-677-964	Molport	0.073	
	Molport-053-294-107	Molport	0.073	
	Z3346257703	Enamine	0.073	
	Z1268451786	Enamine	0.073	
	Z1567828390	Enamine	0.073	
	Z1317841154	Enamine	0.073	
	Z1349141059	Enamine	0.074	
	Z1252385969	Enamine	0.074	
	Z1754406588	Enamine	0.074	
B	Z1675272972	Enamine	0.073	
	MolPort-010-653-848	Molport	0.075	
	Z1359373165	Enamine	0.077	
	Z1252338047	Enamine	0.077	
	Z1349164618	Enamine	0.082	
	Z1252348704	Enamine	0.089	
	MolPort-045-936-636	Molport	0.092	
	MolPort-010-733-027	Molport	0.11	
	MolPort-010-704-694	Molport	0.111	
	MolPort-006-846-922	Molport	0.111	

MolPort-010-653-848 produced the lowest overall SwissParam score at -9.0428, followed by Z1349141059 at -8.8625 and Z3015295812 at -8.7523. Similar docking scores were

© The National High School Journal of Science 2026

Table 4 Molecular docking results of compounds identified through virtual screening.

Name	Lowest ΔG on Chain A	Lowest ΔG on Chain B	Lowest ΔG (SwissParam)	Image	Image w/ Protein Surface
Z3015295779	-8.3322	-8.5761	-8.5761		
Molport-053-218-951	-7.8363	-7.9923	-7.9923		
MolPort-020-180-030	-6.5164	-6.4490	-6.5164		
Molport-038-946-285	-7.4331	-7.4285	-7.4331		
MolPort-044-191-483	-8.3592	-8.1620	-8.3592		
MolPort-046-064-872	-7.0539	-6.9238	-7.0539		
Z3015295812	-8.4517	-8.7523	-8.7523		
Z4326712495	-7.9896	-7.9119	-7.9896		
Molport-053-217-485	-8.2646	-7.9684	-8.2646		
Molport-053-218-995	-8.6623	-8.2940	-8.6623		
MolPort-020-168-373	-7.0646	-7.0636	-7.0646		
MolPort-035-677-964	-6.3198	-6.2985	-6.3198		
Molport-053-294-107	-6.4342	-6.5044	-6.5044		
Z3346257703	-8.2656	-8.0512	-8.2656		
Z1268451786	-7.0608	-7.0634	-7.0634		
Z1567828390	-7.5513	-7.5217	-7.5513		
Z1317841154	-7.0032	-6.8961	-7.0032		
Z1349141059	-8.8625	-8.4922	-8.8625		
Z1252385969	-8.5048	-8.5573	-8.5573		
Z1754406588	-8.2238	-8.4518	-8.4518		
Z1675272972	-7.9655	-7.8361	-7.9655		
MolPort-010-653-848	-9.0428	-8.6618	-9.0428		
Z1359373165	-8.2157	-8.2772	-8.2772		
Z1252338047	-7.9710	-7.9214	-7.9710		
Z1349164618	-7.8853	-7.9486	-7.9486		
Z1252348704	-8.1487	-8.2481	-8.2481		
MolPort-045-936-636	-7.5297	-7.5169	-7.5297		
MolPort-010-733-027	-8.4589	-8.3005	-8.4589		
MolPort-010-704-694	-7.5848	-7.6832	-7.6832		
MolPort-006-846-922	-7.7437	-7.6727	-7.7437		

observed between chains A and B for the evaluated molecules.

Saracatinib, another known Fyn Kinase inhibitor, was docked using the same protocol as the screened compounds and produced a SwissParam score of -8.2988. Of the 30 screened compounds, 9 compounds produced more favorable SwissParam scores than saracatinib, while 21 produced less favorable scores.

ADME Analysis

The 15 molecules selected from the molecular docking results were tested for their agreement with Lipinski's Rule and ADME properties, as presented in Table 6.

Table 5 Predicted ADME profiles of the 15 molecules with the lowest SwissParam scores. From left to right, the table lists the name, agreement with Lipinski's Rule, BBB permeability, and water solubility for each of the top 15 molecules with the lowest SwissParam scores.

Name	Lipinski's Rule	BBB permeant	Water Solubility
MolPort-010-653-848	Disagree (1 violation: MLOGP>4.15)	Yes	Moderately Soluble
Z1349141059	Agree	No	Moderately Soluble
Z3015295812	Agree	No	Soluble
Molport-053-218-995	Agree	No	Soluble
Z3015295779	Agree	No	Soluble
Z1252385969	Agree	No	Moderately Soluble
MolPort-010-733-027	Agree	Yes	Moderately Soluble
Z1754406588	Agree	No	Soluble
MolPort-044-191-483	Agree	No	Moderately Soluble
Z1359373165	Agree	Yes	Moderately Soluble
Z3346257703	Agree	No	Soluble
Molport-053-217-485	Agree	No	Soluble
Z1252348704	Agree	No	Soluble
Molport-053-218-951	Agree	No	Soluble
Z4326712495	Agree	No	Soluble

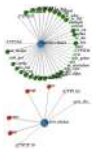
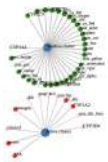
Of the 15 molecules tested, 13 agreed with Lipinski's Rule. The compounds in agreement had 0-2 hydrogen-bond donors, 3-6 hydrogen-bond acceptors, molecular weights ranging from 289.33 to 429.52 g/mol, and CLogP values ranging from 0.09 to 2.78. Their predicted water solubility ranged from moderately soluble to soluble. Of the compounds which agreed with Lipinski's Rule, two were BBB-permeant. Compounds predicted to be BBB-permeant may be compatible with CNS targeting.

© The National High School Journal of Science 2026

Toxicity Analysis

The molecules that demonstrated acceptable ADME properties and BBB permeability were evaluated by finding predicted LD50 values, toxicity classes, toxicity radar charts, and toxicity network charts. Table 7 presents these values for each of the 2 molecules.

Table 6 Toxicity predictions, radar chart metrics, and target network interactions.

Name	LD_{50} (mg/kg)	Toxicity Class	Prediction Accuracy	Data from Radar Chart	Network Chart
MolPort-010-733-027	300	3	54.26%	• **Ecotoxicity:** Molecule: 70%, Avg: 82% • **Respiratory Toxicity:** Molecule: 71%, Avg: 78% • **Neurotoxicity:** Molecule: 85%, Avg: 85% • **CYP2C19:** Molecule: 51%, Avg: 81% • **CYP1A2:** Molecule: 66%, Avg: 82% • **THRβ:** Molecule: 58%, Avg: 79%	
Z1359373165	300	3	67.38%	• **AhR:** Molecule: 71%, Avg: 79% • **Clinical Toxicity:** Molecule: 60%, Avg: 81% • **Ecotoxicity:** Molecule: 68%, Avg: 82% • **Mutagenicity:** Molecule: 72%, Avg: 79% • **Carcinogenicity:** Molecule: 64%, Avg: 80% • **Respiratory Toxicity:** Molecule: 61%, Avg: 78% • **Neurotoxicity:** Molecule: 85%, Avg: 85% • **Hepatotoxicity:** Molecule: 51%, Avg: 82% • **CYP2D6:** Molecule: 56%, Avg: 83% • **CYP1A2:** Molecule: 74%, Avg: 82% • **THRβ:** Molecule: 52%, Avg: 79%	

Key for Network Charts:

- Dark green: Inactive (Probability $>= 0.7$)
- Light green: Inactive (Probability < 0.7)
- Dark red: Active (Probability $>= 0.7$)
- Light red: Active (Probability < 0.7)

Both molecules had a predicted LD50 of 300 mg/kg and were classified as toxicity class 3. Both were also predicted to be active in the neurotoxicity, respiratory toxicity, and ecotoxicity endpoints, as well as CYP1A2 and THRβ.

Discussion

The computational workflow identified several small molecules with favorable predicted interactions with Fyn kinase. DoGSiteScorer identified 23 potential binding sites, with P_7 and P_0 producing the highest drug scores. PrankWeb independently identified three pockets, with Pocket 1 and Pocket 2 receiving substantially higher scores than Pocket 3.

Pharmacophore screening subsequently identified 30 molecules with strong matches to the selected interaction features. Molecular docking further narrowed these candidates based on predicted binding interactions, with MolPort-010-653-848, Z1349141059, and Z3015295812 producing the most favorable SwissParam scores, more favorable predicted docking scores than saracatinib under the same docking protocol. Of the 15 compounds selected for ADME evaluation, two molecules satisfied Lipinski's Rule and were predicted to penetrate the BBB. Toxicity prediction solidified these molecules as computational fits by showing they had acceptable LD50 values of 300 mg/kg and few active toxicity pathways. This allowed for the identification of two computational hits, MolPort-010-733-027 and Z1359373165, based on their low SwissParam scores corresponding to stronger interaction with Fyn kinase, ability to penetrate the BBB, and acceptable toxicity levels in the body.

The results addressed the primary objective of identifying potential small-molecule compounds capable of binding to Fyn kinase. This was accomplished through the systematic narrowing of compounds. The results produced a small group of candidates demonstrating favorable chemical characteristics while also accounting for safety.

Despite the promising computational results, several key limitations should be considered in this experiment. All experiments were conducted using computational models and online servers rather than real experiments. Although these tools are widely used and provide valuable insights, they cannot fully replicate the accuracy of laboratory-based experiments. These experiments therefore require confirmation through experimental methods. Additionally, the scope of the compound search was restricted to the MolPort and Enamine databases, which together only contain just over 10 million commercially available compounds. While this is a substantial amount, it only covers a fraction of potential drug-like molecules. Searching across a wider set of databases could increase the likelihood of finding a compound with better binding to Fyn kinase, acceptable ADME, and less predicted toxicity than our current lead compound.

Although molecular docking identified compounds with favorable predicted binding energies and plausible interactions within the Fyn kinase binding pocket, these computational predictions do not establish target kinase inhibition. Molec-

© The National High School Journal of Science 2026

ular docking assesses whether a molecule could adopt a compatible binding pose within the modeled binding site. Experimental analysis measuring Fyn binding would therefore be necessary to determine whether the computational hits actually inhibit Fyn. Thus the compounds identified in this study should be considered computationally prioritized candidates rather than validated Fyn inhibitors. Similarly, in *silico* counterscreening against off-target kinases was beyond the scope of this study and represents a significant limitation.

This work demonstrates that binding-site prediction, pharmacophore screening, molecular docking, ADME evaluation, and toxicity prediction provides an efficient computational pipeline for identifying promising Fyn kinase inhibitors. Although experimental validation remains necessary, the identified computational hits represent candidates for future medicinal chemistry optimization and biological evaluation.

Acknowledgments

I would like to thank Dr. Moustafa Gabr for guidance, mentorship, and support throughout this research project.

References

1 X. W. Q. Zheng, Alzheimer's disease: insights into pathology, molecular mechanisms, and therapy. Protein Cell. Vol. 16, pg. 83–120, 2025. https://doi.org/10.1093/procel/pwae026.

2 J. Z. W. E. Liu, Y. Zhang, Updates in Alzheimer's disease: from basic research to diagnosis and therapies. Transl Neurodegener. Vol. 13, pg. 45, 2024. https://doi.org/10.1186/s40035-024-00432-x.

3 J. K. J. P. L. P. B. M. B. B. K. Beata, W. J. Wojciech, Alzheimer's disease—biochemical and psychological background for diagnosis and treatment. Int J Mol Sci. Vol. 24, pg. 1059, 2023. https://doi.org/10.3390/ijms24021059.

4 A. P. R. J. K. P. H. R. U. Sehar, P. Rawat, Amyloid Beta in Aging and Alzheimer's Disease. Int J Mol Sci. Vol. 23, pg. 12924, 2022. https://doi.org/10.3390/ijms232112924.

5 P.-V. G. P. G. Castellani RJ, Jamshidi P, The Amyloid Cascade Hypothesis: A Conclusion in Search of Support. The American Journal of Pathology. Vol. 195, pg. 1988–1997, 2025. https://doi.org/10.1016/j.ajpath.2024.10.014.

6 Y. Y. Chen, Tau and neuroinflammation in Alzheimer's disease: interplay mechanisms and clinical translation. J Neuroinflammation. Vol. 20, pg. 165, 2023. https://doi.org/10.1186/s12974-023-02853-3.

7 D. K. K. L. K. V. P. T. Kamatham, R. Shukla, Pathogenesis, diagnostics, and therapeutics for Alzheimer's disease: breaking the memory barrier. Ageing Res Rev. Vol. 101, pg. 102481, 2024. https://doi.org/10.1016/j.arr.2024.102481.

8 H. Hampel *et al.*, The Amyloid-β Pathway in Alzheimer's Disease. Molecular Psychiatry. Vol. 26, pg. 5481–5503, 2021. https://doi.org/10.1038/s41380-021-01249-0.

9 e. a. Yang H, Amyloid β-based therapy for Alzheimer's disease: challenges, successes and future. Signal Transduction and Targeted Therapy. Vol. 8, 2023. https://doi.org/10.1038/s41392-023-01484-7.

10 e. a. Morris M, Hyperphosphorylated tau (p-tau) and drug discovery in the context of Alzheimer's disease and related tauopathies. Frontiers in Molecular Neuroscience. 2023. https://doi.org/10.3389/fnmol.2023.1125354.

11 P. S. A. B. B. M. D. H. R. R. Dhapola, S. S. Hota, Recent advances in molecular pathways and therapeutic implications targeting neuroinflammation for Alzheimer's disease. Inflammopharmacology. Vol. 29, pg. 1669–1681, 2021. https://doi.org/10.1007/s10787-021-00889-6.

12 P. E. L. T.-Y. D. R. Y. L. Deng Q, Wu C, Microglia and Astrocytes in Alzheimer's Disease: Significance and Summary of Recent Advances. Aging and Disease. Vol. 15, pg. 1537–1564, 2024. https://doi.org/10.14336/AD.2023.0907.

13 T. K. N. Balázs, D. Bereczki, Cholinesterase inhibitors and memantine for the treatment of Alzheimer and non-Alzheimer dementias. Ideggyogy Sz. Vol. 74, pg. 379–387, 2021. https://doi.org/10.18071/isz.74.0379.

14 W. LM, New and emerging drug therapies for Alzheimer disease. Australian Prescriber. Vol. 47, pg. 75–79, 2024. https://doi.org/10.18773/austprescr.2024.021.

15 K. C. Turgutalp B, Multi-target drugs for Alzheimer's disease. Trends in Pharmacological Sciences. Vol. 45, pg. 628–638, 2024. https://doi.org/10.1016/j.tips.2024.05.005.

16 J. W. Um *et al.*, Alzheimer amyloid-β oligomer bound to postsynaptic prion protein activates Fyn to impair neurons. Nat Neurosci. Vol. 15, pg. 1227–1235, 2012. https://doi.org/10.1038/nn.3178.

17 D. K. S. Meur, Fyn kinase in Alzheimer's disease: unraveling molecular mechanisms and therapeutic implications. Mol Neurobiol. Vol. 62, pg. 643–660, 2025. https://doi.org/10.1007/s12035-024-04286-2.

18 P. G. Salter MW, Src and Fyn regulation of NMDA receptors in health and disease. Neuropharmacology. Vol. 192, article 108615, 2021. https://doi.org/10.1016/j.neuropharm.2021.108615.

19 S. S. K. E. H. Ahn, Fyn Tyrosine Kinase as Harmonizing Factor in Neuronal Functions and Dysfunctions. International Journal of Molecular Sciences. Vol. 21, pg. 4444, 2020. https://doi.org/10.3390/ijms21124444.

20 X. L. R. C. C. Xu, Y. Tang, Fyn, an important molecule in the brain, is a potential therapeutic target for brain tumours. Front Pharmacol. Vol. 15, pg. 1485919, 2024. https://doi.org/10.3389/fphar.2024.1485919.

21 J. A. O. A. C. S. Demuro, R. M. C. Di Martino, GSK-3β, FYN, and DYRK1A: master regulators in neurodegenerative pathways. Int J Mol Sci. Vol. 22, pg. 9098, 2021. https://doi.org/10.3390/ijms22169098.

22 R. M. M. A. Marotta G, Basagni F, Role of Fyn Kinase Inhibitors in Switching Neuroinflammatory Pathways. Current Medicinal Chemistry. Vol. 29, pg. 4738–4755, 2022. https://doi.org/10.2174/0929867329666211221153719.

23 A. G, Dysfunctional microglia and tau pathology in Alzheimer's disease. Reviews in the Neurosciences. Vol. 34, pg. 443–458, 2023. https://doi.org/10.1515/revneuro-2022-0087.

24 Z. H *et al.*, Interaction between Aβ and Tau in the Pathogenesis of Alzheimer's Disease. International Journal of Biological Sciences. Vol. 17, pg. 2181–2192, 2021. https://doi.org/10.7150/ijbs.57078.

25 e. a. Huang Y, Protein kinases in neurodegenerative diseases: current understandings and implications for drug discovery. Signal Transduction and Targeted Therapy. Vol. 10, 2025. https://doi.org/10.1038/s41392-025-02179-x.

26 M. Bugnon *et al.*, SwissDock 2024: major enhancements for small-molecule docking with Attracting Cavities and AutoDock Vina. Nucleic Acids Res. Vol. 52, 2024. https://doi.org/10.1093/nar/gkae300.

27 M. B. V. Z. U. F. Röhrig, M. Goullieux, Attracting Cavities 2.0: improving the flexibility and robustness for small-molecule docking. J Chem Inf

© The National High School Journal of Science 2026

Model. Vol. 63, 2023. https://doi.org/10.1021/acs.jcim.3c00054.

28 J. S. Delaney, ESOL: estimating aqueous solubility directly from molecular structure. J Chem Inf Comput Sci. Vol. 44, pg. 1000–1005, 2004. https://doi.org/10.1021/ci034243x.

© The National High School Journal of Science 2026